Response of Saos-2 osteoblast-like cells to laser surface texturing, sandblasting and hydroxyapatite coating on CoCrMo alloy surfaces

Batal, Afif; Sammons, Rachel; Dimov, Stefan

DOI:
10.1016/j.msec.2019.01.067

Document Version
Peer reviewed version

Citation for published version (Harvard):
Batal, A, Sammons, R & Dimov, S 2019, 'Response of Saos-2 osteoblast-like cells to laser surface texturing, sandblasting and hydroxyapatite coating on CoCrMo alloy surfaces', *Materials Science and Engineering C*, vol. 98, pp. 1005-1013. https://doi.org/10.1016/j.msec.2019.01.067

Published in Materials Science and Engineering: C
https://doi.org/10.1016/j.msec.2019.01.067

Response of Saos-2 osteoblast-like cells to laser surface texturing, sandblasting and hydroxyapatite coating on CoCrMo alloy surfaces

A. Batal[1], R. Sammons[2], S. Dimov[1]

[1] *Department of Mechanical Engineering, University of Birmingham, Edgbaston, Birmingham, B15 2TT, UK*
[2] *School of Dentistry, University of Birmingham, Edgbaston, Birmingham, B5 7EG, UK*

Abstract:

Cobalt chrome alloys are commonly used in orthopaedic implants where high stiffness and wear resistance are required. This study proposes Laser Surface Texturing (LST) as a cost-effective mean for producing bioinspired surface textures in order to improve the performance of CoCrMo orthopaedic implants. Cobalt-chrome alloy disks were modified using three different LST strategies: i) micro-scale texturing using a nanosecond laser source; (ii) micro-scale texturing with an ultrashort laser source and (iii) bioinspired sub-micron scale texturing with an ultrashort laser source. The modified disks were characterized and compared to blasted, hydroxyapatite coated and polished surface finishes. Saos-2 osteoblast-like cells were seeded on the different surfaces and their proliferation and morphology was assessed. The laser modification increases the surface energy of the CoCrMo alloy disks when compared to their untreated counterparts. The bioinspired sub-micron textured surfaces exhibited the highest cell metabolic activity on day 7 of the MTT assay.

1. Introduction

Cobalt-chrome alloys are widely used by the medical device industry especially as orthopaedic implant materials. They were first introduced in the 1930s owing to their remarkable corrosion resistance, biocompatibility and excellent mechanical properties [1]. Due to their high stiffness and superior wear-resistance, cobalt-chrome alloys are used instead of titanium alloys in high stress applications such as scoliosis rods and bearing surfaces [2,3]. Moreover, the most popular total knee arthroplasty (TKA) design, accounting for 36% of all the TKAs performed in 2009 in England and Wales in 2009, was redesigned in 2006 changing the implant material from titanium to cobalt-chrome based alloy [4,5]. The objective of this change was to minimize the polyethylene insert wear (backside wear), and to increase implant success and life expectancy [5]. Early clinical results showed survival rates of 96.6% with revision for any reason and 98.6% with revision for aseptic failure at 5 years postoperative [6]. These results were very encouraging when compared to the previous titanium design which recorded a 97.2% success rate for any revision at five years and a 99.5% rate for aseptic failure. Now, cobalt-chrome alloys are also commonly used in dental prosthetics, due to their fatigue resistance and retaining capabilities and they are the material of choice for many removable partial dentures [7,8]. However the alloy's remarkable hardness makes it difficult to machine using conventional processes [9].

Although cobalt chrome alloys outperform titanium in stiffness and wear resistance, concerns have been raised about cobalt toxicity. In particular, adverse effects caused by wear debris were reported in patients with CoCrMo metal-on-metal bearing systems [10]. Therefore, this is a very active research field and there are continuous developments to improve CoCr alloys' biocompatibility. For example, De Villiers et al. developed silver chromium nitride coatings for cobalt-chrome bearing surfaces and their use led to less wear while negligible cobalt was released when compared to their uncoated counterparts [11].

Hydroxyapatite (HA) coatings are widely used in industry to improve uncemented stem survival [12,13]. Although coatings may help to improve the performance of CoCrMo orthopaedic implants, there are several limitations associated with their broad use, i.e. high manufacturing costs, potential failures at the interfaces and detrimental interactions with physiological fluids [14]. Also, it is worth mentioning that the benefits of these coatings are still questionable [15].

In recent years, bio-inspired hierarchical micro/sub-micron topographies have shown potential to improve bioactivity and biocompatibility of implant materials. Sousa et al. demonstrated that bio-inspired freestanding multilayer membranes produced via a layer-by-layer technique, enhanced the adhesive properties of natural-based polymers [16]. Wang et al. showed that self-assembled TiO_2 nanotubes on a hierarchical micro/nano titanium surface lead to superior attachment and growth of osteoblasts when compared with a smooth machined Ti surface [17]. Li et al. produced microwell arrays inspired by the surface of rose petals to enhance the contact between polyester and fibroblasts [18]. Such intricate structures are commonly fabricated via complex, difficult to control and expensive chemical processes which limit their commercial viability. Furthermore, most studies were conducted on polymers and titanium.

Laser surface texturing (LST) has attracted the interest of researchers and industry in the last fifteen years, mostly due its tribology applications. Many studies reported the benefits of LST in friction and wear reduction that led to commercial applications of the technology for cylinder liner honing and mechanical seals [19]. The non-contact nature of laser processing makes it an attractive tool to process and modify the otherwise hard to machine cobalt-chrome alloys.

More recently, LST has attracted significant interest as a surface modification technology with potential applications in orthopaedic implants. LST-based surface modifications were reported to reduce the risk of aseptic failures of implants and also to strengthen the bond between the bone and implant by promoting bone cell proliferation and attachment [20, 21, 22, 23]. Mariscal-Muñoz et al. cultured primary osteoblast cells on laser-modified (roughening) Ti surfaces and demonstrated increased ALPase activity and mineralised nodule formation together with enhanced expression of mature bone cell phenotypical markers in comparison with polished Ti surfaces [24]. Furthermore, Shah et al. demonstrated that the Nd:YAG laser modifications (roughening) of commercially pure titanium implants increased the removal torque (RTQ) in rabbit tibiae by 153% when compared to machined implants. The higher RTQ was attributed to the strength of the bone-implant interface; laser-treated implants showed fracture lines at 30 to 50 µm from the interface when tested for failure, whereas separation occurred at the bone-implant interface for the machined surfaces [25].

Many researchers stated that implant surface energy plays a significant role in the interactions of the implant with biological fluids, cells and tissues. In particular, hydrophilic surfaces were reported to promote osseointegration and implant anchorage [26, 27, 28, 29, 30, 31]. However, such surface functionalities are commonly achieved by means of toxic gases [32], harmful chemicals or expensive coating procedures [33, 34, 35]. At the same time the use of LST as an alternative solution for producing hydrophilic implant surfaces, which may favour biological interactions, has not been thoroughly examined; in fact, most of the studies reported an opposite (hydrophobic) effect unless the samples had been stored in controlled environments [36, 37, 38, 39, 40, 41].

There is currently limited literature on the use of LST on CoCr alloys to improve surface properties for cell interactions. Qin et al. investigated the effects of LST on CoCrMo alloy wettability and MC3T3-E1 osteoblast-like cells proliferation. However the disjoint micro-scale patterns (circular, rectangular and triangular pits) produced lead to an increase in the water contact angle when compared with untreated surfaces. Moreover, while the duration of the cell incubation was only 48h, no significant difference in the MC3T3-E1 cells proliferation was observed between the different samples [42]. Further work is hence required to study the effects of bio-inspired surface topographies, achievable via LST, on cell attachment and proliferation on cobalt-chrome alloys. This research evaluates the wettability and proliferation of Saos-2 osteoblast-like cells on 3 different types of laser modified CoCrMo alloy surfaces: nanosecond laser structuring, femtosecond laser structuring and sub-micron laser patterning. It also compares their performance with the current state of the art in the implant industry, i.e. blasted and HA coated surfaces, together with polished surfaces as references.

2. Material and Methods

2.1 CoCrMo Samples

A surgical cobalt-chromium-molybdenum casting alloy with the following Wt% composition was used in all experiments: 67.0% Co, 27.0% Cr and 5.0% Mo. Disks with a diameter of 18mm and 2mm thickness were supplied by MatOrtho Ltd. UK. The samples were sandblasted, 20 grit white fused alumina, and some were manually polished on linishing belts down to a mirror finish (Ra < 0.05µm).

2.2 Laser Surface Texturing

Three different LST approaches were investigated as follows: (i) micro-scale texturing employing a nanosecond laser source (NS surfaces) ; (ii) micro-scale texturing with an ultrashort laser source (FS surfaces) and (iii) bioinspired sub-micron scale texturing with an ultrashort laser source (NT surfaces), namely to mimic the corneal surface of some insects such as moths, butterflies and drosophila [43] . The ultrashort laser had the following technical specification (Satsuma from Amplitude Systemes): 5W average power, 10µJ max pulse energy, 310fs pulse duration, up to 500 KHz repetition rate, 1030nm wavelength and a beam quality M^2 better than 1.2. The technical specification of the nanosecond laser source (redENERGY G4 from SPI Lasers) was as follows: 50W average power, 0.71 mJ max pulse energy, pulse durations in the range 15 to 220 ns, up to 1Mhz repetition rate, 1060nm wavelength and beam quality M^2 better than 1.3. The laser spot size was approximately 30 µm in diameter at the focal point for both laser sources.

A grid of 100 x 100 µm grooves with a spacing of 400 µm was chosen as the micro-scale pattern for both NS and FS surfaces. This particular groove size was selected to be similar to the size of Saos-2 cells that is generally just under 100 µm in any direction when adhered and fully spread on a flat surface [44]. The microscale recessions on the surface should offer a favourable environment for the cells to settle, adhere and spread [45]. To better understand the influence of pulse duration on resulting surface topographies, and consequently cell growth, the grids were produced using two different laser sources.

Laser Induced Periodic Surface Structures (LIPSS) have been shown to induce a positive response from osteoblast cells (and osteoblast-like cell lines) on various polymers and titanium alloys. However, the sub-micron ripples tend to influence the orientation and spreading of cells [46]. Thus, this bio-inspired semi-omnidirectional geometry was chosen to produce the NT surfaces in an effort to avoid any directionality.

The NS and FS surfaces were produced on the blasted disks (B). To produce NT surfaces, LST was carried out on mirror finish polished disks (P). The three LST strategies employed to produce NS, FS and NT surfaces are depicted in Fig. 1 while the laser parameters used in the experiments are given in Table 1. These were chosen in order to achieve the desired topographies within minimal processing times. LST was performed in ambient conditions with the assistance of a fume extractor.

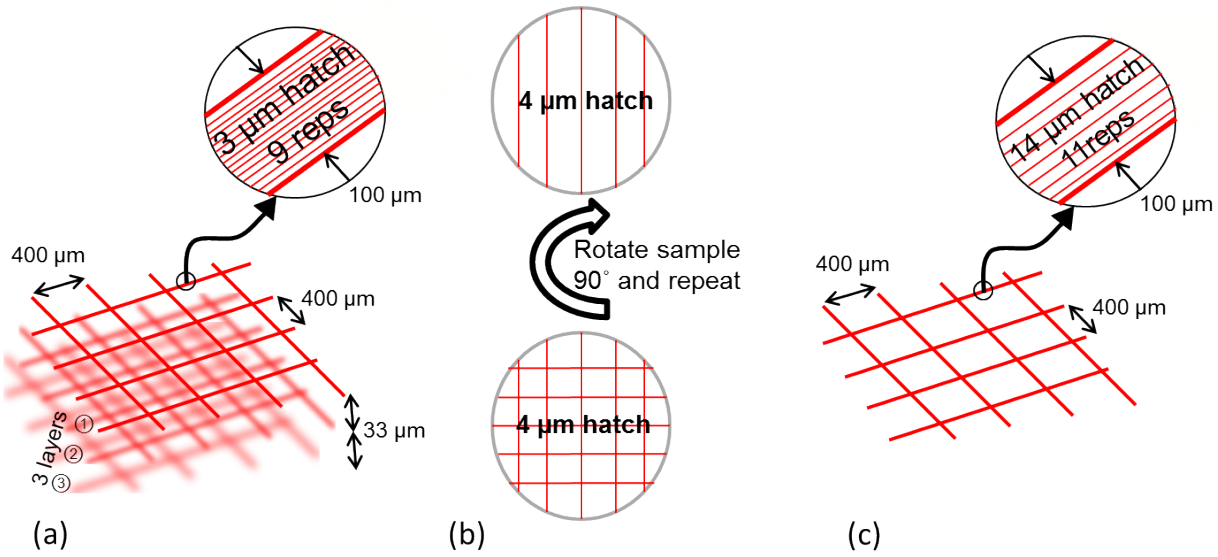

Figure 1. Schematic diagrams of the LST strategies used to produce (a) FS surfaces, (b) NT surfaces and (c) NS surfaces

Note: *hatch* refers to the step-over distance between two consecutive laser scans while *reps* to the number of scanning repetitions per layer.

Sample	Average Power (W)	Pulse Duration	Repetition Rate (kHz)	Scanning Speed (mm/s)
FS	4.19	310 fs	500	1000
NT	1st scan: 0.57/2nd scan: 0.1	310 fs	250	1000
NS	33.4	220 ns	65.5	950

Table 1. Laser parameters used for LST

2.3 Hydroxylapatite Coating

High-purity synthetic calcium hydroxylapatite from Plasma Biotal Ltd. UK was used to coat the blasted disks. Particles 30µm in diameter with a highly crystalline structure (>50%) were deposited on the CoCrMo surface. The coating meets the requirements of ISO 13779:2000 which specifies hydroxyapatite powders that should be used as a raw material for producing surgical implants or their coatings.

2.4 Surface Topography Assessment

Focus variation microscopy, i.e. G5 InfiniteFocus system from Alicona, was used to analyse the 3D surface topographies of the B, NS, FS and HA disks, to assess their surface roughness.

All 6 samples were examined by scanning electron microscopy using a Zeiss EVO MA 10 microscope: WD=6.0mm and EHT=20.00kV.

Sample	Treatment	Original Surface
B	Sand Blasting	Cast
P	Mirror Finish Polishing	Cast
NT	Sub-Micron Texturing Femtosecond Laser	Mirror Finish Polished
FS	Micro Grooves Femtosecond Laser	Blasted
NS	Micro Grooves Nanosecond Laser	Blasted
HA	Hydroxylapatite Coated	Blasted

Table 2. Summary of the tested samples

2.5 Surface Wettability

Contact angle (CA) analysis was performed employing the sessile drop technique, using an Attension Theta optical tensiometer with 4μL drops of Milli-Q water. The measurements were taken 5 and 30 days after LST to assess the impact of disk storage in ambient conditions on the evolution of contact angle and thus to judge the functional stability of created topographies. Before the first measurement the samples underwent rigorous cleaning: The samples were subjected to three 15 min ultrasonic baths, first, in 8 wt% aqueous oxalic acid, second, in pure acetone, and third, in 70 vol% ethanol aqueous solution. The samples were rinsed with distilled pure water in-between baths and finally dried with argon gas.

2.6 Cell Culture

All CoCrMo disks underwent the cleaning protocol described above followed by autoclaving at 120° C 1 bar pressure . Specimens were then placed in 12-well plates (Thermo Scientific™ Nunc™ Cell-Culture Treated Multidishes) and approximately $2x10^4$ Saos-2 osteoblast-like cells were seeded on each sample in McCoy's 5A medium supplemented with 10% FBS, I00U/mL of Penicillin and 100μg/mL of Streptomycin. The well plates were placed in a humidified incubator at 37˚C in an atmosphere of 5% CO_2 and the culture medium was changed every 2 days.

2.7 Cell Proliferation

Saos-2 cells metabolic activity was evaluated via a MTT assay, reflecting the cells' proliferation on the different CoCrMo specimens. MTT was prepared in phosphate buffered saline (PBS, pH 7.4) at a concentration of 5mg/mL. 100μL of the MTT solution was added to each well and the plates were incubated at 37˚C in an atmosphere of 5% CO_2 for 4 hours at the selected time intervals (2, 4 and 7 days). The medium was then removed and 1mL of DMSO was added to each well to dissolve the formazan. The well plates were placed on a shaking platform for 5 minutes and then the optical density was measured at 570nm using a spectrophotometer.

2.8 Cell Morphology

At selected time intervals: 2, 4 and 7 days after seeding, samples were rinsed with phosphate buffered saline (PBS, pH 7.4) and then immersed in 2.5% EM grade glutaraldehyde in 0.1M sodium

cacodylate buffer (pH 7.3) prepared on the day. After fixation, the different CoCrMo disks were then dehydrated by immersion in solutions of increased ethanol concentration: 20, 30, 40, 50, 60, 70, 90, 95 (twice) and 100% (twice). The ethanol was then removed and the disks' surfaces were rinsed with hexamethyldisilzane (HMDS) and left to evaporate in a fume cupboard overnight. Finally the disks were sputter coated with gold and examined under SEM to image the attached cells on the surface.

2.9 Statistical Analysis

All data was expressed as means with their standard deviations. Contact angle average values were calculated based on 5 measurements on each disk while the average MTT optical density values based on 3 measurements. Statistical analysis was performed using Minitab 17 Statistical Software. General Linear Model ANOVA was used to examine differences between the groups. Values of $p<0.05$ were considered significant.

3. Results and Discussion

3.1 Focus Variation Microscopy

The surface topographies of the B, FS, NS and HA specimens are depicted in Fig. 2.

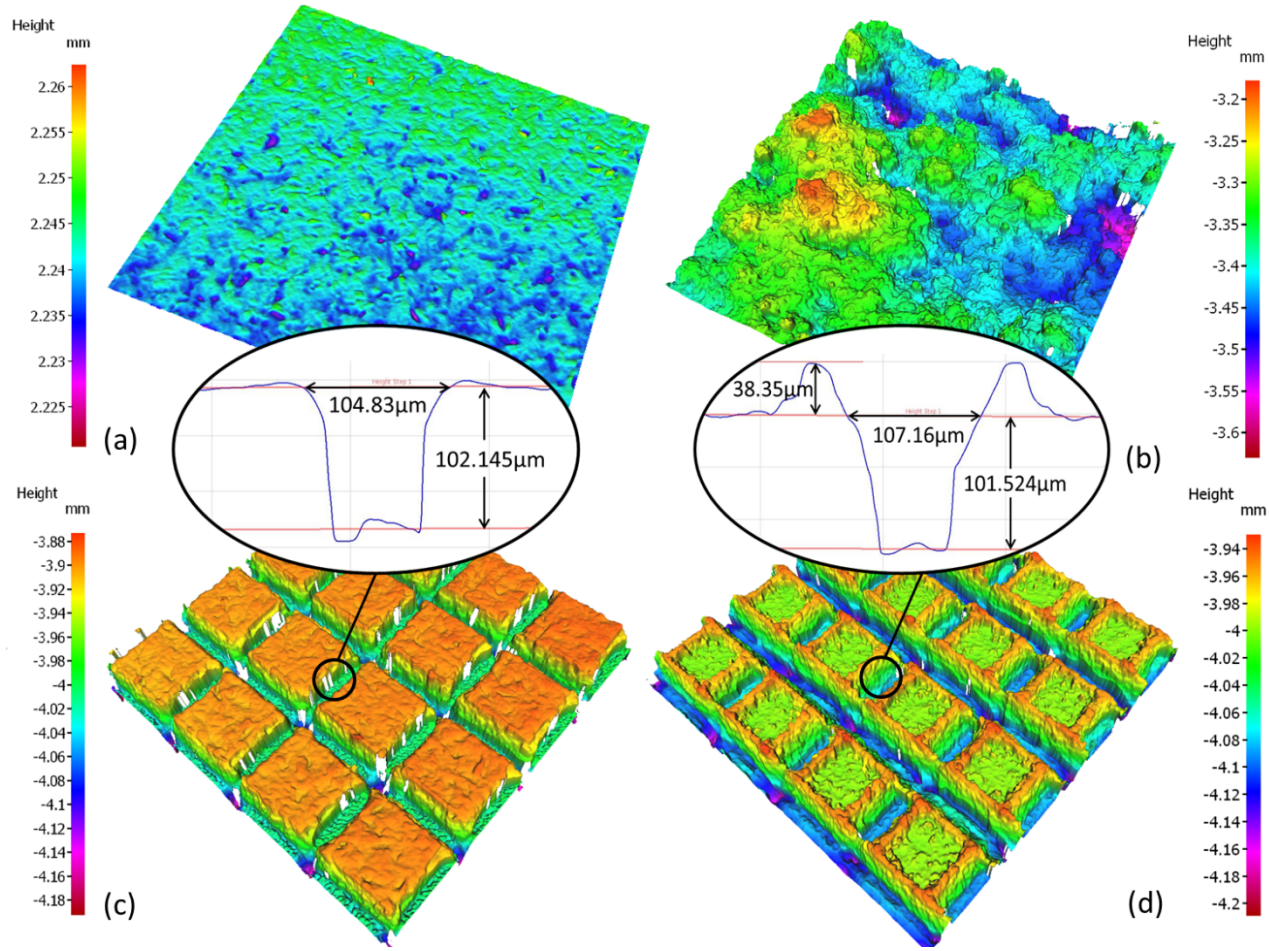

Figure 2. Topography measurements of (a) B surface (b) HA surface (c) FS surface (d) NS surface

The 3D surface profiles were made with the 10x objective of the Alicona G5 microscope. Using the same magnification, the arithmetical mean height (S_a) and root mean square height (S_q) values of the blasted and HA coated specimens were calculated over a 1.62mm^2 area. The S_a and S_q values for the B surface were 60.02µm and 60.11µm, respectively, compared with 89.61µm and 106.3µm for the HA coated surface, making it the roughest surface by a significant margin with values higher than the 100µm deep grooves of the NS and FS surfaces. As for the NT surface, the S_a and S_q values were measured using the 100x objective over a 0.0256mm^2 area and they were 0.05µm and 0.07µm respectively, a slight increase over the mirror finish.

The desired groove width and depth was produced with both FS and NS laser sources with deviations less than 10%. However, the resulting topographies differ considerably; the longer pulse duration used for the NS samples resulted in a significant recast bulges along the grid edges of the CoCrMo disks that enclosed non-processed areas in-between the grooves. Furthermore, after producing the grooves in one direction, the processing of perpendicular grooves to form the grids resulted in re-deposition of molten material where they intersected the existing ones.

In contrast, due to the nature of ultrashort pulsed laser processing that is also commonly referred to as “cold ablation”, no recast budges were observed on the FS disks. The non-processed area retained its blasted finish characteristics while the grooves’ intersection remained open in both directions.

Additionally, the grooves of the NS surfaces exhibited a larger draft angle when compared to the almost-vertical walls obtained along the FS grooves, which could be attributed to the higher thermal load when longer pulses were used and consequently a high amont of molted material and slashes along the groves.

3.2 Scanning Electron Microscopy

The SEM micrographs of all 6 investigated surfaces are presented in Fig. 3.

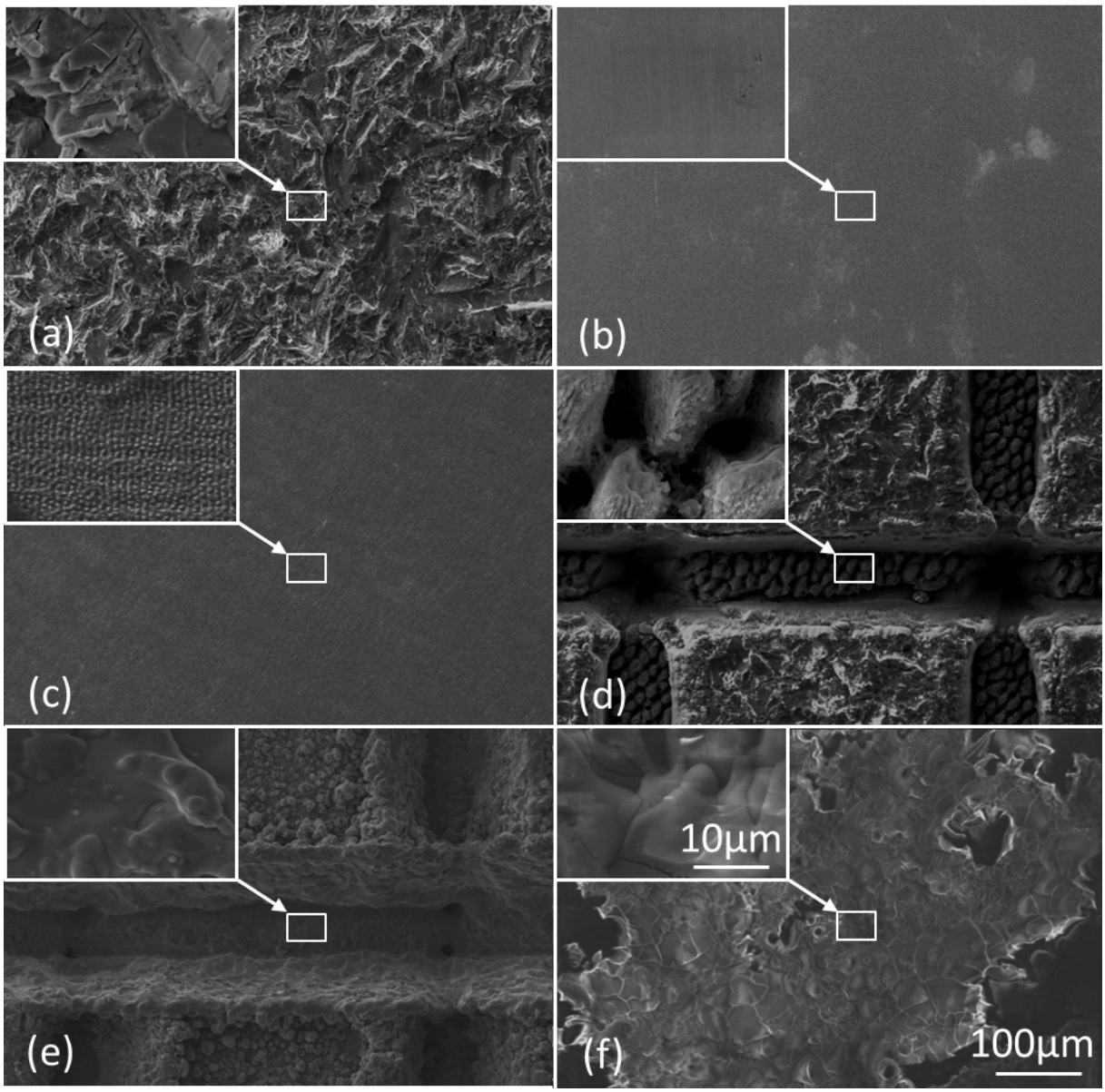

Figure 3. SEM micrographs of: (a) B surface; (b) P surface; (c) NT surface; (d) FS surface; (e) NS surface and (f) HA surface.

Scale bars are valid for all images.

It is evident that apart from the NT and P surfaces, the CoCrMo disks have a significant roughness. The B surface had uniform roughness whereas the FS, NS and HA surfaces were more irregular as seen from both the SEM images and focus variation microscopy. The difference between the NS and FS surfaces is depicted in more detail in Fig. 4. Regarding the NT surface, a hexagonal sub-micron array resembling the corneal surface of insects was successfully formed on the initially polished surface (Fig. 4d windowed). The distance between two consecutive sub-micron features is just under the wavelength of the ultrashort laser source used: 600-700nm in this case. This has been thoroughly documented when producing LIPSS with an ultrashort pulsed laser [47]. Nano bumps

were formed instead of linear ripples due to the 90° rotation of the samples between the first and second scans together with the use of lower power in the second scan, and as a result the ripples from the two scans intersected to form the nano-bumps. It is important to stress that the power settings in the two scans are very important to generate this particular NT surfaces. In particular, if the second scan is performed with the same laser power, the first set of ripples will be erased while no LIPSS would be generated if the power settings are too low. The energy levels should thus be just sufficent to ablate the peaks of the first set of LIPSS, giving this particular bio-inspired sub-micron topography.

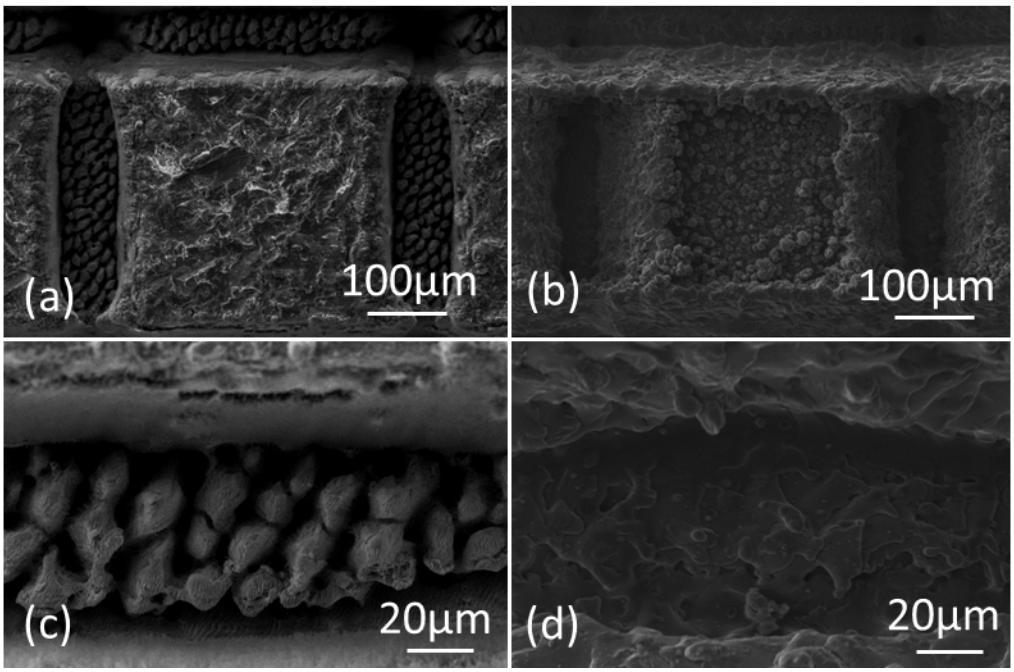

Figure 4. SEM micrographs of (a) FS surface (b) NS surface (c) FS groove (d) NS groove

The differences between the FS and NS surfaces, especially the effects of the 2 different pulse durations, are depicted in more detail in Fig. 4. In particular, the unprocessed areas between the grooves of the NS samples are covered with re-solidified molten CoCrMo while the recast bulges are very prominent at the intersections, even closing the first set of grooves, and also along the edges, as can also be seen in Fig. 2. In contrast, the untreated areas of the FS samples retained their blasted surface characteristics, no recast formations along the grooves were observed and the first set of grooves was only narrowed at the intersections. Taking a closer look at the bottom of the grooves (Fig. 4c & d), it can be seen that the processed surface areas with the longer 220ns pulses were re-melted and smoothened whereas a self-organised hierarchical micro/nano morphology was observed in the FS groove as a result of multiple passes, in particular the accumulated laser fluence [48]. The morphology is of similar scale to that of the rose petals examined by Li et al. [18], nano ripples can be observed on the top of the micro features that measure between 15 and 20 µm.

3.3 Surface Wettability

The contact angle (CA) values are shown in Fig. 5.

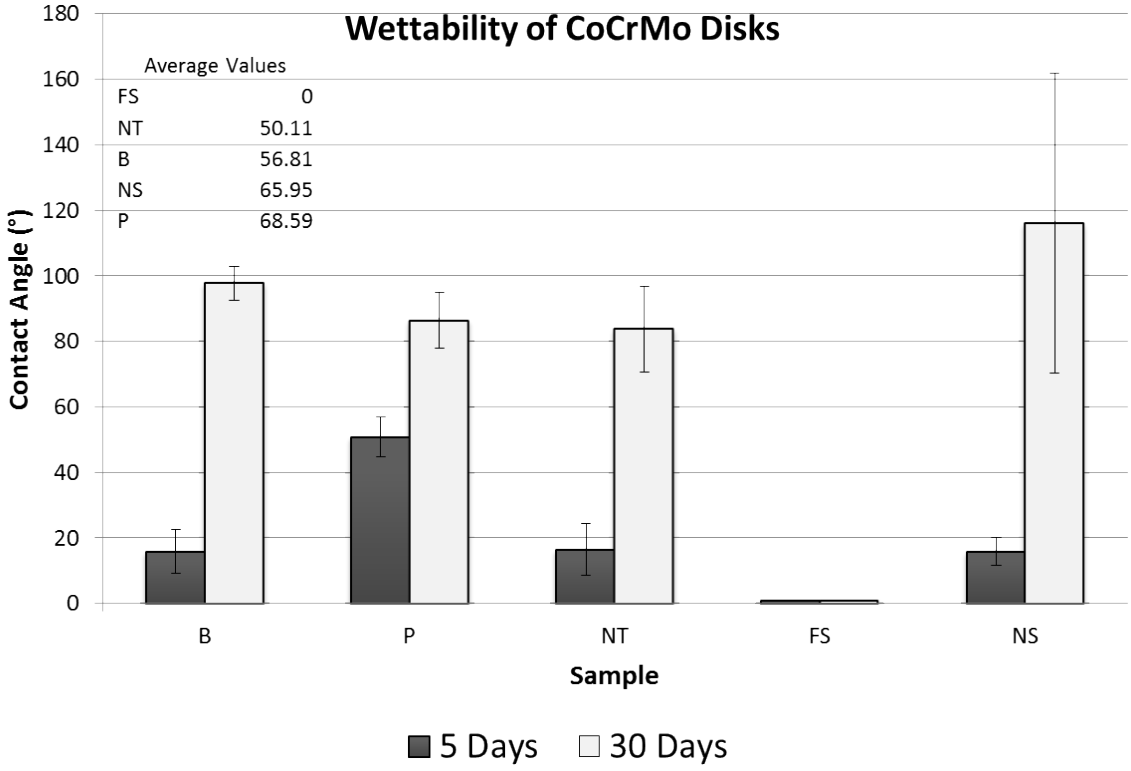

Figure 5. Contact angle of the different uncoated CoCrMo surfaces

Looking at the average CA values 5 days after laser texturing, all samples were hydrophilic, with 0° CA for the FS sample processed with the ultrashort laser, while the CA values for the NS, NT and B samples were similar at ~15°, only the polished disks exhibited a higher CA at ~50°. With time (30 days), all CA values increased except for the FS sample. This increase in CA values has been observed by many researchers and is commonly attributed to changes in surface chemistry [49, 50].

Furthermore, the large CA deviation of NS samples after 30 days is due to the directional nature of the surface. In fact, the samples exhibited semi-hydrophilic properties in the direction of the open grooves and were hydrophobic in the direction of the closed ones while the value in Fig. 5. is the average of both. This is due to some capillary effects that have led to droplets spreading in the direction of the open grooves. However, the droplets still did not flow inside the grooves as reflected by the lowest contact angle of 70˚. Luo et al. [51] argued that the cell-like structures (unprocessed areas enclosed by the molten material) repel the water droplets due to some entrapped air. Thus, the NS surface exhibits a mixed Cassie-Baxter (CB) - Wenzel wetting state, especially a transitional state between CB and Wenzel regimes, similar to the one seen with pigeon feathers [52].

On the other hand, the FS samples exhibited a complete Wenzel state of wetting where there was complete contact between the liquid and the solid surface, reflected by the contact angle of 0˚. This wetting state can be attributed to the lack of ‘air pockets’ due to the absence of molten material

around the edges of the grooves and the morphology at the bottom of the grooves that prevented the air being compressed as it is open to the environment [53].

3.4 Saos-2 Cell Proliferation and Morphology

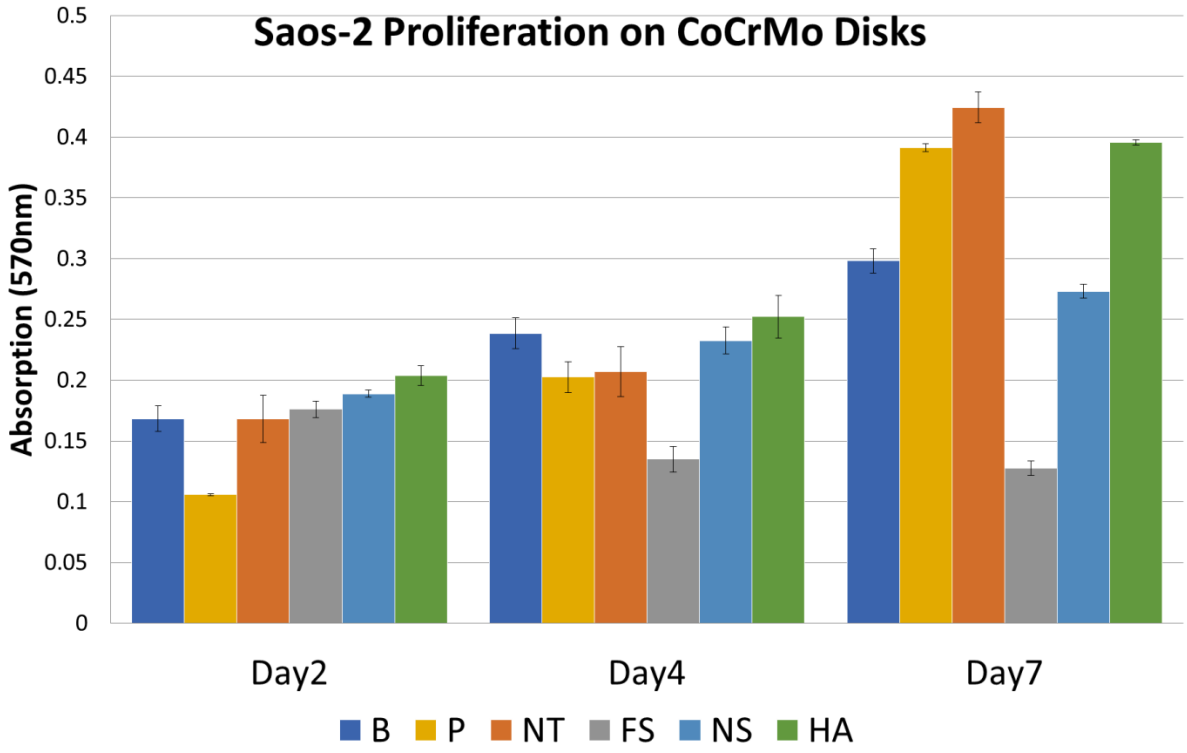

Figure 6. Proliferation of Saos-2 cells on the 6 different CoCrMo surfaces after 2, 4 and 7 days. (n=3, statistical significance indicated by $p<0.05$)

From the MTT assay, a number of conclusions can be drawn. Initial cell adhesion is favourable on surfaces with a significant roughness, this is reflected in the higher cell metabolic activity on the B, FS, NS and HA surfaces when compared to the P on Day2. However, the rate of proliferation is much in favour of surfaces with low S_a values. In fact, the P and NT samples exhibited the highest rates of proliferation at 93.21% and 105.1%, respectively, between Day4 and Day7. In contrast, cells on the hydroxyapatite coated disk increased by 56.84% in the same time period. This phenomenon was also seen with epithelial cells on different titanium surfaces [54]. This could be attributed to the mechanical micro-anchorage of the cells onto the disks with micro-topography. The NT surface exhibited high levels of initial adhesion, comparable to those of the four rough surfaces (B, FS, NS, HA), yet it also showed the highest rate of proliferation between Day4 and Day7. This highlights the important role of sub-micron features in terms of cell adhesion.

At the end of the assay on Day7, the Sub-micron Textured CoCrMo disk showed the highest cell metabolic activity.

From the ANOVA, it can be concluded that the topography is a very significant factor with a p-value of 0.001<<<0.05. As for the contribution percentages, they are 29.15 and 39.10% for the factors Topography and Day respectively.

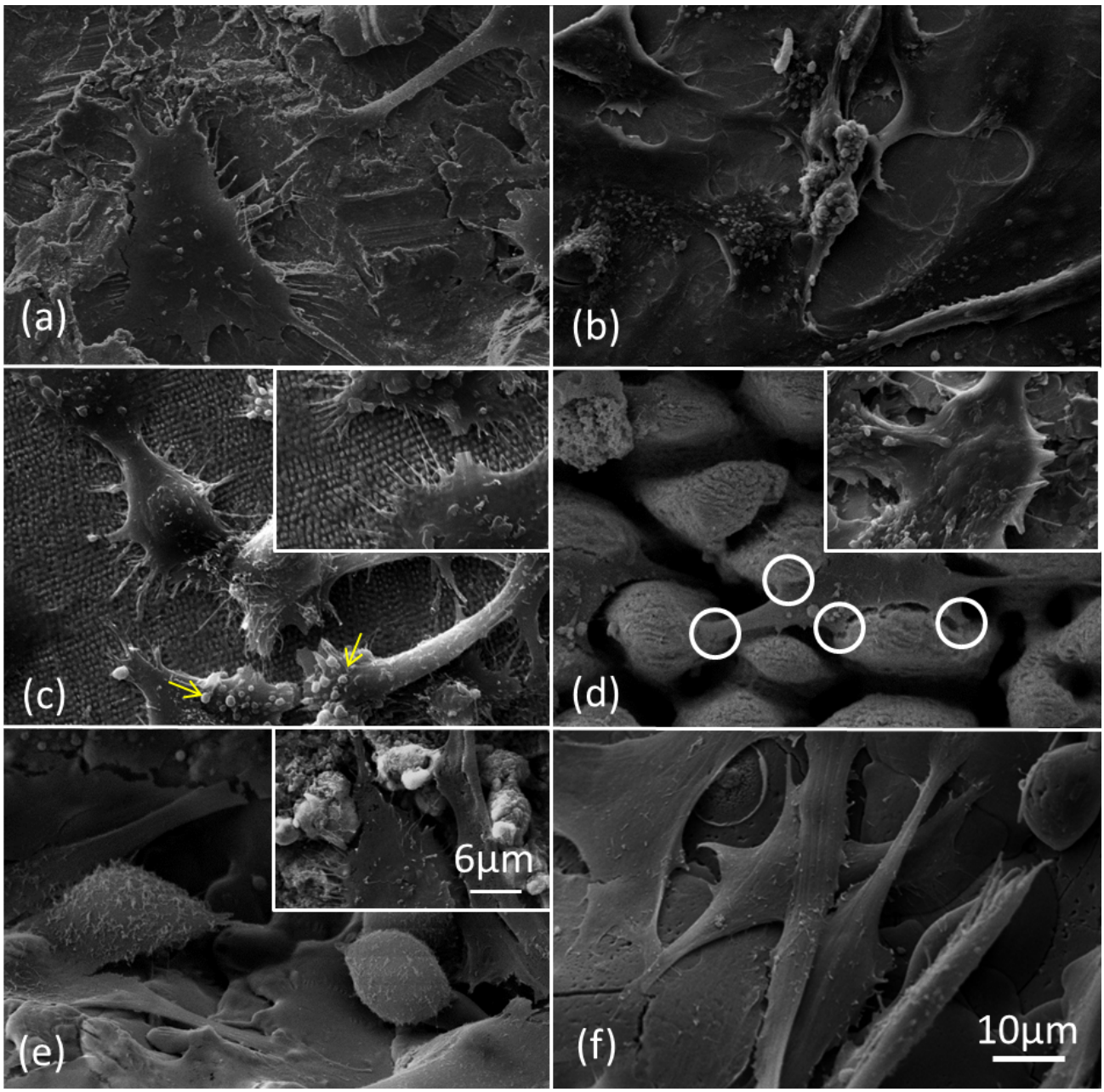

Figure 7. Representative SEM micrographs of Saos-2 cells at day 4 on: (a) B surface; (b) P surface; (c) NT surface; (d) FS surface; (e) NS surface and (f) HA surface.

Scale bars are valid for all images.

Cell adhesion and proliferation was monitored by SEM at day 4 (Fig. 7). Cells were not confluent at this time on any of the surfaces except for the HA surface (Fig. 7f). On the B surface (Fig. 7a) the Saos-2 cells were relatively flat on the sample but less spread than in the P samples, as was seen on Titanium surfaces by Degasne et al. [55]. In some areas of the P surface (Fig. 7b) the cells appeared almost confluent and were completely flattened and spread out on the surface with few exceptions,

as is typical of such surfaces [55]. On the NT surface (Fig. 7c) the cells had a raised profile and several filopodia can be seen attached to the nanofeatures (Fig. 7c windowed). Blebs (arrows) were seen in the cell membrane of many cells on this surface, which could be indicative of secretive metabolic activity. The filopodia anchoring the cells to the sub-micron topography explains the high initial adhesion on Day2 unlike the P surfaces. Moreover, the cells on this surface did not show signs of directionality, as was hypothesised, which is otherwise common with LIPSS surfaces [46]. On the FS surface (Fig. 7d) there was no cell growth inside the grooves and only occasional cells were seen, as pictured, spanning the hierarchical features. Cells in the untextured areas had the same characteristics as on the blasted surface (Fig. 7d windowed and Fig. 7a). On the NS surface (Fig. 7e) the cells were concentrated in the grooves as expected, which could be attributed to some capillary action of the cell media, but a few cells were also present on the untreated area, they had a similar morphology to those found on the B surfaces (Fig. 7e windowed). On the HA surface (Fig. 7f) the cells appeared elongated and there appeared to be more than one cell layer developing.

Both B and NS surfaces showed similar levels of proliferation and comparable morphologies. This suggests that the anchoring and growth mechanisms are similar on both surfaces with micro-topography.

Generally, higher growth was expected on the HA surfaces compared to uncoated metallic surfaces. Okumura et al. reported that Saos-2 cells settled and differentiated earlier on HA compared to pure titanium [56]. This was indeed the case with the CoCrMo alloy samples as well, especially a higher growth and adhesion was seen on the HA samples on Day2 and Day4.

The differences in water contact angle and cell attachment between the FS and NS samples can therefore be attributed to the hierarchical structures at the bottom of the FS grooves and the splashes of molten material. Those differences led to changes in the wetting states, i.e. Cassie-Wenzel for the NS samples and Wenzel for the FS samples, and thus there was no correlation between CA and cell attachment in this case. However, there is some correlation between the surface response on the P and NT surfaces. Especially, the P and NT surfaces exhibited almost identical wetting behaviours owing to their comparable surface roughness values and thus high hydrophilicity let to a greater attachment and proliferation.

Osteoblast cells have been seen to grow across grooves much wider than the distance between 2 consecutive hierarchical structures seen in the FS grooves. In fact, De Luca et al. reported that primary osteoblast cells grew across 40µm wide grooves on the surface of 316 L austenitic stainless steel [57]. This indicates that the morphology of the hierarchical structures, and not the distance in between them, caused the cell growth inhibition. Moreover the cells' points of contact were seen almost exclusively on the side of the hierarchical structures (Fig. 7d, circles) which could indicate that the cells could not attach to the top of the said structures.

4. Conclusions

Six different CoCrMo samples with different surface topography were studied for osteoblast-like Saos-2 cell morphology and proliferation. In particular, the cell responses after applying three different laser texturing procedures were compared to those obtained on blasted and polished specimens and also samples with a commercially-used hydroxyapatite coating. The following conclusions were made based on the obtained results:

1. Saos-2 cell adhesion occurred on all the CoCr surfaces and the surface topography was an important factor governing both cell morphology and proliferation.
2. A higher roughness encourages initial cell adhesion however smoother/planner surfaces facilitate cell proliferation.
3. The highest metabolic activity occurred on Day 7 on the NT surface, as shown by the MTT assay. This can be attributed to both the anchoring effects of the sub-micron textures and also the high proliferation levels of smooth surfaces. In addition, the cells on the NT samples that had bio-inspired sub-micron topography did not show any signs of directionality.
4. Surface topography is a more significant factor than surface energy in Saos-2 cell attachment and proliferation. Controlling the micron (cell size) and sub-micron scales of implant surfaces could lead to much improved biological responses.
5. Correlation between CA and cell proliferation is only valid when both the wetting behaviours and surface roughness values are comparable.
6. Long lasting super hydrophilic, 0˚ CA, surfaces can be produced via ultrashort pulsed laser structuring, namely by producing micro grooves with hierarchical micro/nano topography at the bottom, FS samples.
7. Saos-2 cells grew in the micro-grooves produced with the longer 220ns laser pulses but not in the ones produced with the ultrashort pulses, in fact the FS grooves inhibited cell attachment and growth. This suggests that the self-organized hierarchical micro/nano structures found in the FS grooves could be used to potentially control cell migration.

Based on the findings in this research, it can be argued that the potential ideal CoCrMo implant surface should be a combination of micro-scale structures and sub-micro features. In particular, the micro-scale structures would facilitate both the mechanical anchorage with the bone and also offer a better initial osteoblast cell adherence, while the smooth surfaces with sub-micron features would improve proliferation and growth without compromising adherence. Such surfaces can be produced simultaneously by employing femtosecond laser sources and thus to selectively modify implants both at the micro and sub-micro scales in one processing step.

5. Acknowledgments

The research reported in this paper was carried out in collaboration with MatOrtho Ltd. and was supported by two European Commission H2020 projects, i.e. the ITN programme “European ESRs Network on Short Pulsed Laser Micro/Nanostructuring of Surfaces for Improved Functional Applications” (Laser4Fun) and the FoF programme “High-Impact Injection Moulding Platform for mass-production of 3D and/or large micro-structured surfaces with Antimicrobial, Self-cleaning, Anti-scratch, Anti-squeak and Aesthetic functionalities” (HIMALAIA). In addition, the work was carried out within the framework of the UKIERI DST programme “Surface functionalisation for food, packaging, and healthcare applications”.

References

[1] Chen, Q., & Thouas, G. A. (2015). Metallic implant biomaterials. *Materials Science and Engineering: R: Reports*, *87*, 1-57.

[2] Shinohara, K., Takigawa, T., Tanaka, M., Sugimoto, Y., Arataki, S., Yamane, K., ... & Sarai, T. (2016). Implant failure of titanium versus cobalt-chromium growing rods in early-onset scoliosis. *Spine*, *41*(6), 502-507.

[3] Serhan, H., Mhatre, D., Newton, P., Giorgio, P., & Sturm, P. (2013). Would CoCr rods provide better correctional forces than stainless steel or titanium for rigid scoliosis curves?. *Clinical Spine Surgery*, *26*(2), E70-E74.

[4] Anon., "National Joint Registry for England and Wales Summary to the 7th Annual Report," 2009. Retrieved from http://www.njrcentre.org.uk/

[5] Anon., "Johnson and Johnson. Company Literature and Marketing," PFC Sigma Cobalt-Chrome, Leeds, 2010. Retrieved from https://www.depuysynthes.com/

[6] Wood, A. M., Heil, K. M., Brenkel, I. J., & Walmsley, P. (2018). Press fit condylar cobalt chrome sigma total knee arthroplasty: No difference to original design at five year point. Journal of Arthroscopy and Joint Surgery, 5(1), 15-18.

[7] Vallittu, P. K., & Kokkonen, M. (1995). Deflection fatigue of cobalt-chromium, titanium, and gold alloy cast denture clasp. *The Journal of Prosthetic Dentistry*, *74*(4), 412-419.

[8] Savitha, P. N., Lekha, K. P., & Nadiger, R. K. (2015). Fatigue resistance and flexural behavior of acetal resin and chrome cobalt removable partial denture clasp: an in vitro study. *European Journal of Prosthodontics*, *3*(3), 71.

[9] Zaman, H. A., Sharif, S., Kim, D. W., Idris, M. H., Suhaimi, M. A., & Tumurkhuyag, Z. (2017). Machinability of Cobalt-based and Cobalt Chromium Molybdenum Alloys-A Review. Procedia Manufacturing, 11, 563-570.

[10] Delaunay, C., Petit, I., Learmonth, I. D., Oger, P., & Vendittoli, P. A. (2010). Metal-on-metal bearings total hip arthroplasty: the cobalt and chromium ions release concern. *Orthopaedics & Traumatology: Surgery & Research*, *96*(8), 894-904.

[11] De Villiers, D., Banfield, S., Housden, J., & Shelton, J. (2016). Silver Chromium Nitride Coatings On Cobalt Chrome Alloy To Reduce Cobalt Ion Release And Prevent Infections. *Bone Joint J*, *98*(SUPP 7), 108-108.

[12] Friedman, R. J., Bauer, T. W., Garg, K., Jiang, M., An, Y. H., & Draughn, R. A. (1995). Histological and mechanical comparison of hydroxyapatite-coated cobalt-chrome and titanium implants in the rabbit femur. *Journal of Applied Biomaterials*, *6*(4), 231-235.

[13] Lacefield, W. R. (1988). Hydroxyapatite coatings. *Annals of the New York academy of sciences*, *523*(1), 72-80.

[14] Nimb, L., Gotfredsen, K., & Steen Jensen, J. (1993). Mechanical failure of hydroxyapatite-coated titanium and cobalt-chromium-molybdenum alloy implants. An animal study. *Acta orthopaedica belgica*, *59*, 333-333.

[15] Hailer, N. P., Lazarinis, S., Mäkelä, K. T., Eskelinen, A., Fenstad, A. M., Hallan, G., ... & Kärrholm, J. (2015). Hydroxyapatite coating does not improve uncemented stem survival after total hip arthroplasty! An analysis of 116,069 THAs in the Nordic Arthroplasty Register Association (NARA) database. *Acta orthopaedica*, *86*(1), 18-25.

[16] Sousa, M. P., & Mano, J. F. (2017). Cell-adhesive bioinspired and catechol-based multilayer freestanding membranes for bone tissue engineering. Biomimetics, 2(4), 19.

[17] Wang, F., Shi, L., He, W. X., Han, D., Yan, Y., Niu, Z. Y., & Shi, S. G. (2013). Bioinspired micro/nano fabrication on dental implant–bone interface. Applied Surface Science, 265, 480-488.

[18] Li, P., Dou, X., Feng, C., & Schönherr, H. (2018). Enhanced cell adhesion on a bio-inspired hierarchically structured polyester modified with gelatin-methacrylate. *Biomaterials science*, *6*(4), 785-792.

[19] Etsion, I. (2005). State of the art in laser surface texturing. *Transactions of the ASME-F-Journal of Tribology*, *127*(1), 248.

[20] Liu, X., Chu, P. K., & Ding, C. (2004). Surface modification of titanium, titanium alloys, and related materials for biomedical applications. *Materials Science and Engineering: R: Reports*, *47*(3), 49-121.

[21] Mendonça, G., Mendonça, D. B., Aragao, F. J., & Cooper, L. F. (2008). Advancing dental implant surface technology–from micron-to nanotopography. *Biomaterials*, *29*(28), 3822-3835.

[22] Klokkevold, P. R., Nishimura, R. D., Adachi, M., & Caputo, A. (1997). Osseointegration enhanced by chemical etching of the titanium surface. A torque removal study in the rabbit. *Clinical oral implants research*, *8*(6), 442-447.

[23] Cho, S. A., & Jung, S. K. (2003). A removal torque of the laser-treated titanium implants in rabbit tibia. *Biomaterials*, *24*(26), 4859-4863.

[24] Mariscal-Muñoz, E., Costa, C. A., Tavares, H. S., Bianchi, J., Hebling, J., Machado, J. P., ... & Souza, P. P. (2016). Osteoblast differentiation is enhanced by a nano-to-micro hybrid titanium surface created by Yb: YAG laser irradiation. *Clinical oral investigations*, *20*(3), 503-511.

[25] Shah, F. A., Johansson, M. L., Omar, O., Simonsson, H., Palmquist, A., & Thomsen, P. (2016). Laser-modified surface enhances osseointegration and biomechanical anchorage of commercially pure titanium implants for bone-anchored hearing systems. *PloS one*, *11*(6), e0157504.

[26] Buser, D., Broggini, N., Wieland, M., Schenk, R. K., Denzer, A. J., Cochran, D. L., ... & Steinemann, S. G. (2004). Enhanced bone apposition to a chemically modified SLA titanium surface. *Journal of dental research*, *83*(7), 529-533.

[27] Zhao, G., Schwartz, Z., Wieland, M., Rupp, F., Geis-Gerstorfer, J., Cochran, D. L., & Boyan, B. D. (2005). High surface energy enhances cell response to titanium substrate microstructure. *Journal of biomedical materials research Part A*, *74*(1), 49-58.

[28] Schwarz, F., Ferrari, D., Herten, M., Mihatovic, I., Wieland, M., Sager, M., & Becker, J. (2007). Effects of surface hydrophilicity and microtopography on early stages of soft and hard tissue integration at non-submerged titanium implants: an immunohistochemical study in dogs. *Journal of periodontology*, *78*(11), 2171-2184.

[29] Vlacic-Zischke, J., Hamlet, S. M., Friis, T., Tonetti, M. S., & Ivanovski, S. (2011). The influence of surface microroughness and hydrophilicity of titanium on the up-regulation of TGFβ/BMP signalling in osteoblasts. *Biomaterials*, *32*(3), 665-671.

[30] Le Guéhennec, L., Soueidan, A., Layrolle, P., & Amouriq, Y. (2007). Surface treatments of titanium dental implants for rapid osseointegration. *Dental materials*, *23*(7), 844-854.

[31] Wennerberg, A., Jimbo, R., Stübinger, S., Obrecht, M., Dard, M., & Berner, S. (2014). Nanostructures and hydrophilicity influence osseointegration: a biomechanical study in the rabbit tibia. *Clinical oral implants research*, *25*(9), 1041-1050.

[32] Niino, H., & Yabe, A. (1993). Surface modification and metallization of fluorocarbon polymers by excimer laser processing. *Applied Physics Letters*, *63*(25), 3527-3529.

[33] Okabe, Y., Kurihara, S., Yajima, T., Seki, Y., Nakamura, I., & Takano, I. (2005). Formation of super-hydrophilic surface of hydroxyapatite by ion implantation and plasma treatment. *Surface and Coatings Technology*, *196*(1), 303-306.

[34] Zhong, H., Hu, Y., Wang, Y., & Yang, H. (2017). TiO2/silane coupling agent composed of two layers structure: A super-hydrophilic self-cleaning coating applied in PV panels. *Applied energy*, *204*, 932-938.

[35] Rupp, F., Scheideler, L., Olshanska, N., De Wild, M., Wieland, M., & Geis-Gerstorfer, J. (2006). Enhancing surface free energy and hydrophilicity through chemical modification of microstructured titanium implant surfaces. *Journal of Biomedical Materials Research Part A*, *76*(2), 323-334.

[36] Kenar, H., Akman, E., Kacar, E., Demir, A., Park, H., Abdul-Khaliq, H., ... & Karaoz, E. (2013). Femtosecond laser treatment of 316L improves its surface nanoroughness and carbon content and promotes osseointegration: An in vitro evaluation. *Colloids and Surfaces B: Biointerfaces*, *108*, 305-312.

[37] Raimbault, O., Benayoun, S., Anselme, K., Mauclair, C., Bourgade, T., Kietzig, A. M., ... & Donnet, C. (2016). The effects of femtosecond laser-textured Ti-6Al-4V on wettability and cell response. *Materials Science and Engineering: C*, *69*, 311-320.

[38] Fadeeva, E., Truong, V. K., Stiesch, M., Chichkov, B. N., Crawford, R. J., Wang, J., & Ivanova, E. P. (2011). Bacterial retention on superhydrophobic titanium surfaces fabricated by femtosecond laser ablation. *Langmuir*, *27*(6), 3012-3019.

[39] Bizi-Bandoki, P., Benayoun, S., Valette, S., Beaugiraud, B., & Audouard, E. (2011). Modifications of roughness and wettability properties of metals induced by femtosecond laser treatment. *Applied Surface Science*, *257*(12), 5213-5218.

[40] Kietzig, A. M., Hatzikiriakos, S. G., & Englezos, P. (2009). Patterned superhydrophobic metallic surfaces. *Langmuir*, *25*(8), 4821-4827.

[41] Mirhosseini, N., Crouse, P. L., Schmidth, M. J. J., Li, L., & Garrod, D. (2007). Laser surface micro-texturing of Ti–6Al–4V substrates for improved cell integration. *Applied surface science*, *253*(19), 7738-7743.

[42] Qin, L., Zeng, Q., Wang, W., Zhang, Y., & Dong, G. (2014). Response of MC3T3-E1 osteoblast cells to the microenvironment produced on Co–Cr–Mo alloy using laser surface texturing. *Journal of materials science*, *49*(6), 2662-2671.

[43] Blagodatski, A., Sergeev, A., Kryuchkov, M., Lopatina, Y., & Katanaev, V. L. (2015). Diverse set of Turing nanopatterns coat corneae across insect lineages. Proceedings of the National Academy of Sciences, 112(34), 10750-10755.

[44] Pautke, C., Schieker, M., Tischer, T., Kolk, A., Neth, P., Mutschler, W., & Milz, S. (2004). Characterization of osteosarcoma cell lines MG-63, Saos-2 and U-2 OS in comparison to human osteoblasts. *Anticancer research*, *24*(6), 3743-3748.

[45] Lee, M. H., Oh, N., Lee, S. W., Leesungbok, R., Kim, S. E., Yun, Y. P., & Kang, J. H. (2010). Factors influencing osteoblast maturation on microgrooved titanium substrata. *Biomaterials*, *31*(14), 3804-3815.

[46] Rebollar, E., Frischauf, I., Olbrich, M., Peterbauer, T., Hering, S., Preiner, J., ... & Heitz, J. (2008). Proliferation of aligned mammalian cells on laser-nanostructured polystyrene. *Biomaterials*, *29*(12), 1796-1806.

[47] Bonse, J., Krüger, J., Höhm, S., & Rosenfeld, A. (2012). Femtosecond laser-induced periodic surface structures. Journal of Laser Applications, 24(4), 042006.

[48] Nayak, B. K., & Gupta, M. C. (2010). Self-organized micro/nano structures in metal surfaces by ultrafast laser irradiation. Optics and Lasers in Engineering, 48(10), 940-949.

[49] Garcia-Giron, A., Romano, J. M., Liang, Y., Dashtbozorg, B., Dong, H., Penchev, P., & Dimov, S. S. (2018). Combined surface hardening and laser patterning approach for functionalising stainless steel surfaces. *Applied Surface Science*, *439*, 516-524.

[50] Bizi-Bandoki, P., Valette, S., Audouard, E., & Benayoun, S. (2013). Time dependency of the hydrophilicity and hydrophobicity of metallic alloys subjected to femtosecond laser irradiations. *Applied Surface Science*, *273*, 399-407.

[51] Luo, B. H., Shum, P. W., Zhou, Z. F., & Li, K. Y. (2010). Surface geometrical model modification and contact angle prediction for the laser patterned steel surface. *Surface and Coatings Technology*, *205*(7), 2597-2604.

[52] Bormashenko, E., Bormashenko, Y., Stein, T., Whyman, G., & Bormashenko, E. (2007). Why do pigeon feathers repel water? Hydrophobicity of pennae, Cassie–Baxter wetting hypothesis and Cassie–Wenzel capillarity-induced wetting transition. *Journal of colloid and interface science*, *311*(1), 212-216.

[53] Ran, C., Ding, G., Liu, W., Deng, Y., & Hou, W. (2008). Wetting on nanoporous alumina surface: transition between Wenzel and Cassie states controlled by surface structure. *Langmuir*, *24*(18), 9952-9955.

[54] Cochran, D. L., Simpson, J., Weber, H. P., & Buser, D. (1994). Attachment and growth of periodontal cells on smooth and rough titanium. *International Journal of Oral & Maxillofacial Implants*, *9*(3).

[55] Degasne, I., Basle, M. F., Demais, V., Hure, G., Lesourd, M., Grolleau, B., ... & Chappard, D. (1999). Effects of roughness, fibronectin and vitronectin on attachment, spreading, and proliferation of human osteoblast-like cells (Saos-2) on titanium surfaces. *Calcified tissue international*, *64*(6), 499-507.

[56] Okumura, A., Goto, M., Goto, T., Yoshinari, M., Masuko, S., Katsuki, T., & Tanaka, T. (2001). Substrate affects the initial attachment and subsequent behavior of human osteoblastic cells (Saos-2). *Biomaterials*, *22*(16), 2263-2271.

[57] De Luca, A. C., Zink, M., Weidt, A., Mayr, S. G., & Markaki, A. E. (2015). Effect of microgrooved surface topography on osteoblast maturation and protein adsorption. Journal of Biomedical Materials Research Part A, 103(8), 2689-2700.